

# Tailoring Intercalant Assemblies at the Graphene–Metal Interface

Johannes Halle\*, Nicolas Néel, Jörg Kröger

Institut für Physik, Technische Universität Ilmenau, D-98693 Ilmenau, Germany

E-mail: johannes.halle@tu-ilmenau.de

*This document is the unedited Author's version of a Submitted Work that was subsequently accepted for publication in Langmuir, copyright ©American Chemical Society and the Division of Chemical Education, Inc., after peer review. To access the final edited and published work see*

*<https://pubs.acs.org/articlesonrequest/AOR-k9bCzvtT3V6WRd3q4UUw>*

## Abstract

The influence of graphene on the assembly of intercalated material is studied using low-temperature scanning tunneling microscopy. Intercalation of Pt under monolayer graphene on Pt(111) induces a substrate reconstruction that is qualitatively different from the lattice rearrangement induced by metal deposition on Pt(111) and, specifically, the homoepitaxy of Pt. Alkali metals Cs and Li are used as intercalants for monolayer and bilayer graphene on Ru(0001). Atomically resolved topographic data reveal that at elevated alkali metal coverage ( $2 \times 2$ )Cs and ( $1 \times 1$ )Li intercalant structures form with respect to the graphene lattice.

## Introduction

Superstructures at surfaces are ubiquitous.<sup>1,2</sup> They may occur as reconstructions of the clean surface, as an ordered assembly of adsorbates, as a moiré pattern due to the lattice mismatch between adsorbate and substrate lattice or as an electronic superlattice.

In the case of adsorbates, superlattices form as the result of the balance between adsorbate–adsorbate and adsorbate–substrate interactions. Exemplarily, when the adsorbate–adsorbate interaction is dominant characteristic molecular patterns may occur,<sup>3–5</sup> while a stronger adsorbate–substrate coupling may be exploited for template effects, such as the guided adsorption on vicinal surfaces,<sup>6–14</sup> on molecular platforms,<sup>15,16</sup> and on moiré lattices.<sup>17–39</sup> Adsorbate–substrate interactions mediated by surface state electrons<sup>40–45</sup> and electronic moiré patterns<sup>46</sup> were demonstrated to steer the adsorbate assembly as well.

The impetus to the work presented here was the addition of a third interaction and the exploration of a possible further tailoring of surface structures. To this end, graphene-covered metal surfaces, Pt(111) and Ru(0001), and the intercalation of Pt and alkali metals (Cs, Li)

were used. The intercalated material experiences the coupling to the substrate as well as to the graphene. Pt intercalation under graphene on Pt(111) leads to a reconstruction of the Pt surface, which is related to the structures reported for homoepitaxial growth of Pt on pristine Pt(111). However, the presence of graphene induces a considerably extended long-range order of the reconstruction as well as a qualitative change in the underlying dislocation network. For Cs and Li intercalation on graphene-covered Ru(0001) alkali metal assemblies form with respect to the graphene lattice rather than to the metal substrate.

## Experimental Methods

The experiments were performed in ultrahigh vacuum ( $10^{-9}$  Pa) with a scanning tunneling microscope (STM) operated at 5 K. Surfaces of Pt(111) and Ru(0001) were cleaned by repeated  $\text{Ar}^+$  bombardment and annealing at 1200 K in  $\text{O}_2$  atmosphere ( $4 \cdot 10^{-5}$  Pa). Graphene was prepared on the clean surfaces by thermal decomposition of  $\text{C}_2\text{H}_4$ . On Ru(0001) a second layer of graphene was formed by segregation of bulk C.<sup>47</sup> Metal intercalation was performed by, first, depositing Pt from a hot filament, Cs and Li from commercial dispensers onto the respective metal surfaces at room temperature and, second, by annealing the sample at 1200 K (Pt), 660 K (Cs), 570 K (Li). Using this preparation protocol leads to the efficient intercalation of the deposited material, as previously shown for Cs,<sup>48</sup> Li,<sup>49,50</sup> and Ni.<sup>50</sup> The annealing after deposition is particularly important for Cs and Pt since otherwise adsorbed clusters remain on graphene.<sup>25,48,51</sup> The intercalation is further evidenced by the concomitant weakening of the graphene moiré pattern as well as by STM images showing the atomically resolved graphene lattice. Cointercalation proceeded *via* the deposition of Li onto Cs-intercalated graphene on Ru(0001), followed by annealing. STM tips were fabricated from pure Au wire and trained *in situ* by annealing and field emission on a Au substrate. Topographic data were acquired with constant current and the bias voltage applied to the sample. STM images were processed using WSxM.<sup>52</sup>

## Results and Discussion

### Pt(111)

Annealing Pt(111) at temperatures exceeding 1330 K induces a hexagonal reconstruction of the surface.<sup>53,54</sup> STM studies showed that exposing Pt(111) to Pt vapor stabilizes a similar reconstruction already at 400 K, which resembles a honeycomb network of protruding lines.<sup>55</sup> These characteristic superstructures consist of domains where the bulk face-centered cubic (fcc) stacking is retained alternating with hexagonal close-packed (hcp) stacking regions. More recent calculations using the Frenkel-Kontorova model<sup>56</sup> showed that Pt(111) indeed teeters at the brink of a stability domain and may be triggered to reconstruct by small environmental changes.<sup>57</sup> The Pt(111) reconstruction is related to the soliton reconstruction of Au(111)<sup>58-61</sup> and likewise occurs upon deposition of Co,<sup>62</sup> Cr,<sup>63</sup> Cu<sup>64</sup> on Pt(111).

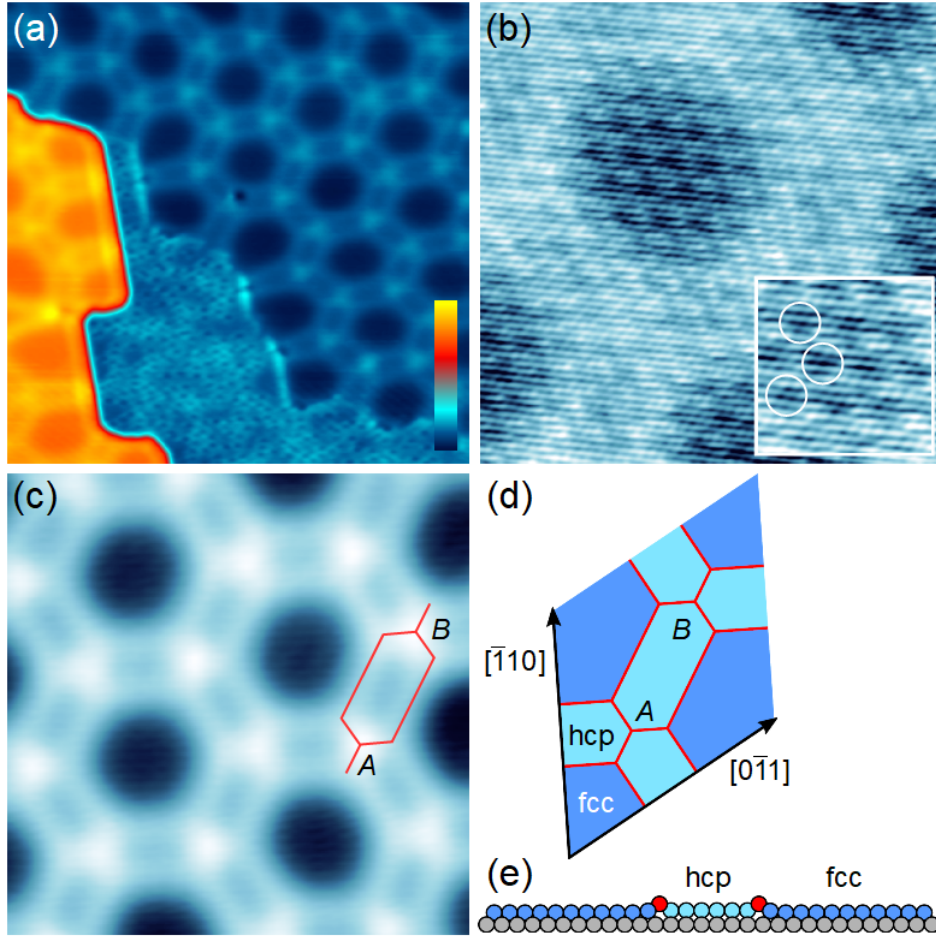


Figure 1: (Color online) Reconstruction of graphene-covered Pt(111) after Pt intercalation. (a) STM image of Pt-intercalated graphene on Pt(111) (bias voltage  $V = 1$  V, tunneling current  $I = 100$  pA, size:  $40 \times 40$  nm<sup>2</sup>). Two adjacent Pt(111) terraces are visible. The honeycomb network is due to a reconstruction of the Pt(111) surface. (b) Atomically resolved close-up view of (a) showing the graphene lattice with parts of the reconstruction ( $50$  mV,  $100$  pA,  $12 \times 12$  nm<sup>2</sup>). Inset: Close-up view of (b) with circles indicating a moiré pattern ( $3.5 \times 3.5$  nm<sup>2</sup>). (c) STM image of the Pt(111) reconstruction network showing the characteristic fcc (hexagonal dark depressions), hcp (stripelike depressions enclosed by bright double lines) stacking domains ( $1$  V,  $100$  pA,  $19 \times 19$  nm<sup>2</sup>). The triangle-shaped bright protrusions are the connectors of the network (see text). (d) Illustration of structural elements of the reconstruction network. Regions with hcp stacking are separated from fcc domains by pairs of lines that are oriented along  $[11\bar{2}]$ ,  $[1\bar{2}1]$ ,  $[\bar{2}11]$  directions. The double lines intersect at  $A$  and  $B$ . (e) Side view of first and second Pt(111) atomic layer along  $\langle \bar{1}10 \rangle$ . 30 surface Pt atoms reside atop 29 second-layer Pt atoms giving rise to fcc and hcp stacking regions with protruding double lines.

Here, possible modifications of this reconstruction due to the presence of graphene are investigated. Figure 1a shows a representative STM image of two adjacent terraces of graphene-covered Pt(111) after Pt intercalation. Most obvious is a regular honeycomb superstructure that extends over a few hundred nanometers. It is characterized by a spatial period of  $7.99 \pm 0.08$  nm with parallel ridges separated by  $1.98 \pm 0.10$  nm. This superstructure is assigned to a reconstruction of the Pt(111) surface due to its resemblance to previously reported reconstructions on that surface.<sup>53,55</sup> In particular, the ridges will be referred to as double lines following conventional phrasing.<sup>55,65</sup> Deviating from the rather irregular network of double lines observed from the reconstruction induced by the homoepitaxial growth of Pt on clean Pt(111)<sup>55,65</sup> the presence of graphene apparently causes a regular and extended honeycomb reconstruction pattern. Before analyzing the superstructure in more detail two remarks are noteworthy. First, the STM image of Figure 1a shows that regions without reconstruction may occur. A surface area on the lower terrace and close to a substrate edge does not exhibit a reconstructed surface. Second, the presence of monolayer graphene (MLG) can be inferred from the atomically resolved graphene lattice (Figure 1b). As indicated by the circles in the inset to Figure 1b, a moiré pattern with a spatial period of  $1.00 \pm 0.02$  nm is visible. The angle between the moiré and graphene lattice is  $1.2^\circ \pm 1.1^\circ$ , which is in accordance with the angle of  $14.5^\circ \pm 0.7^\circ$  enclosed by graphene and the Pt(111) lattice. This graphene lattice orientation is observed on both reconstructed and unreconstructed surface regions since graphene spans these regions without discontinuity (Figure 1a). A second orientation was observed on Pt(111) with a smaller spatial period of  $0.79 \pm 0.02$  nm and an angle of  $-17.5^\circ \pm 0.8^\circ$  enclosed by the graphene and Pt lattices. These moiré patterns are characteristic for MLG on Pt(111).<sup>66,67</sup> The rather low number of graphene orientations observed here is probably due to the rather high annealing temperature used for the intercalation of the Pt atoms, which is in agreement with a previous report.<sup>66</sup>

Figure 1c presents topographic data that unravel the structural elements of the observed reconstruction. The illustrations in Figures 1d,e help identify crystallographic directions and surface regions with different stackings. The double lines represent a pair of Shockley partial dislocations that separate hexagonal fcc stacking domains from smaller and elongated hcp-stacked regions.<sup>55,65</sup> Thus, across a pair of Shockley partial dislocations one additional Pt atom is incorporated into the surface, which increases the surface atom density. In the one-dimensional illustration (Figure 1e) 30 surface Pt atoms reside on top of 29 second-layer Pt atoms along  $\langle \bar{1}10 \rangle$  directions.

The arrangement of double lines in the honeycomb reconstruction leads to an isotropic compression of the Pt(111) surface. Previously, double lines were demonstrated to meet in two different manners leading to two different types of dislocation line connectors, the so-called bright and dark stars.<sup>55,65</sup> Bright stars are protruding intersections of three pairs of double lines, where central Pt atoms reside at on-top sites of Pt(111). They provide an energy gain by the annihilation of three point dislocations, which outweighs the energy costs for the accompanying stacking faults.<sup>55,65</sup> Dark stars represent connectors that enclose extended hcp-stacked regions.<sup>55,65</sup> Bright and dark stars reflect the threefold symmetry of Pt(111), which is due to the inequivalence of hcp and fcc sites. Indeed, in all previous reports the energy difference between hcp and fcc sites established a topological law that

forces the two types of connectors – bright and dark stars – to alternate at the corners of the honeycomb hexagons.<sup>56,57,65</sup> The experimental findings reported here (Figure 1) invalidate the topological law since the honeycomb reconstruction surprisingly exhibits protrusions at all connector sites of the dislocation network, labeled *A* and *B* in Figure 1c,d. A possible origin of this observation is discussed next.

The additional interaction of Pt surface atoms with graphene counteracts their coupling to the substrate, which facilitates the reconstruction. A similar argument was put forward to explain the stability of the high-temperature Pt/Pt(111) reconstruction. In this case, a weaker bonding of the Pt surface layer was attributed to thermally excited vibrations.<sup>53,54,57</sup> A second important consequence of the attraction between Pt and graphene is the reduction of stacking-dependent energy differences, especially between hcp and fcc sites. This aspect is corroborated by the remarkably large ratio of hcp-stacked to fcc-stacked areas, which is  $\approx 0.78$  in the case presented here. In comparison, the purely temperature-induced reconstruction of Pt(111) at 1330 K yielded a hcp to fcc ratio of only 0.43.<sup>53,54</sup> Additional deposition of Pt, however, may further enhance this ratio. This was demonstrated in the homoepitaxial growth of Pt on Pt(111) at 400 K yielding a hcp to fcc ratio of  $\approx 0.54$ .<sup>55,65</sup> Since the energy differences between the different stacking sites are reduced due to the presence of graphene, intralayer interactions become more important. Indeed, the strict alternation of bright and dark stars is overcome and the formation of bright stars as connectors of the observed reconstruction network is observed at all six double line intersections of a hexagon. This hints at a preference of bright stars over dark stars in the presence of graphene due to a lower formation energy. The above discussion unravels another important aspect that clarifies the role of graphene in the surface reconstruction. Graphene captures the intercalated Pt close to the substrate. The presence of Pt vapor was previously demonstrated to facilitate the reconstruction.<sup>55,65</sup>

## Ru(0001)

The adsorption of alkali metals on surfaces has a longstanding tradition in surface science.<sup>68–70</sup> The promotion of catalytic reactions<sup>71–74</sup> and the increase of electron emission rates<sup>75</sup> belong to the appealing alkali-induced effects. It is therefore not surprising that many aspects of alkali metal adsorption have been studied, *e. g.*, the geometric structure of superlattices,<sup>76–81</sup> vibrational quanta,<sup>82–85</sup> and lifetimes of electronic excitations<sup>86–92</sup> On graphene, adsorption of alkali metals was shown to, *e. g.*, tune the band gap opening between the graphene Dirac cones<sup>93,94</sup> and modify the electronic transport.<sup>95,96</sup>

More recently, the intercalation of alkali metals on graphene-covered surfaces has moved into a focus of surface science research. For instance, doping of graphene on Ir(111) may be controlled by the intercalation of Cs.<sup>97</sup> In addition, the prediction of superconductivity in Li-decorated free-standing graphene<sup>98</sup> has sparked investigations into electronic<sup>99,100</sup> and structural<sup>49</sup> as well as vibrational<sup>50</sup> properties.

In this section, structural aspects of Cs, Li-intercalated graphene on Ru(0001) are discussed. Figure 2a shows an STM image of MLG and bilayer graphene (BLG) on Ru(0001). The pronounced superlattice is due to a moiré pattern that results from the strong MLG–Ru(0001) hybridization.<sup>101–103</sup> The moiré superlattice of MLG exhibits a spatial period of

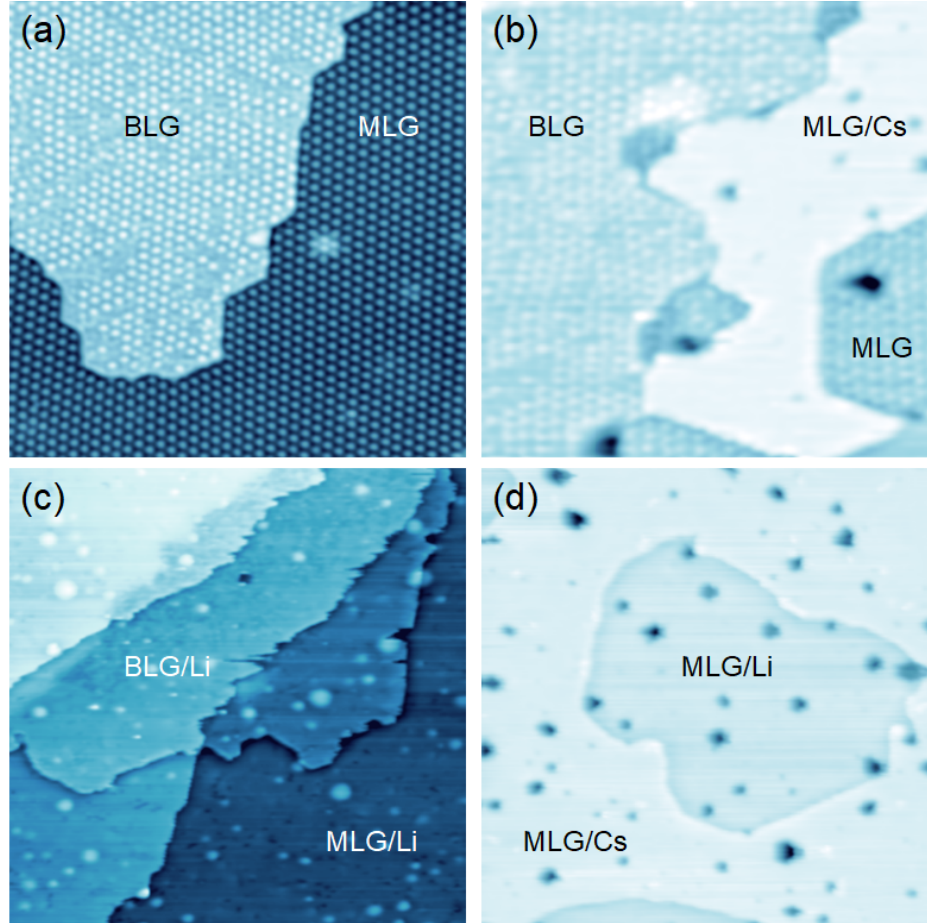


Figure 2: (Color online) Cs and Li intercalation phases on graphene-covered Ru(0001). (a) Monolayer (MLG) and bilayer (BLG) graphene on clean Ru(0001) (200 mV, 100 pA,  $120 \times 120 \text{ nm}^2$ ). The hexagonal superstructure is due to a moiré pattern. (b) Cs-intercalated graphene (MLG/Cs) between MLG and BLG domains (200 mV, 80 pA,  $90 \times 90 \text{ nm}^2$ ). (c) Li-intercalated graphene (300 mV, 100 pA,  $300 \times 300 \text{ nm}^2$ ). Both MLG and BLG are intercalated and labeled as MLG/Li and BLG/Li, respectively. The intercalated regions in (b) and (c) show an essentially vanishing moiré pattern. (d) Cointercalation of Cs and Li (200 mV, 90 pA,  $180 \times 180 \text{ nm}^2$ ). The separate intercalation phases are indicated.

$3.02 \pm 0.05$  nm, in agreement with previous reports.<sup>104–109</sup> The strong MLG buckling of  $112 \pm 4$  pm mainly reflects the actual topography<sup>101,109,110</sup> caused by the hybridization of graphene  $\pi$ -states with Ru  $d$ -bands.<sup>101,105</sup> The angle enclosed by the moiré and MLG lattice is  $4.1^\circ \pm 1.0^\circ$ , which corresponds to a calculated angle of  $0.37^\circ \pm 0.09^\circ$  between the MLG and Ru(0001) lattice. The MLG spatial period and the moiré twist angles reflect an MLG lattice constant of 0.248 nm, which corresponds to a 0.6% tensile stress in MLG. Similar conclusions have been drawn from earlier experimental work and density functional calculations.<sup>101,104,107–109,111</sup>

BLG flakes (Figure 2a) exhibit typical diameters of a few 100 nm and are observed to span several substrate terraces. Often, they occur at Ru(0001) step edges. BLG domains display a moiré pattern with a spatial period of  $2.95 \pm 0.06$  nm and an angle of  $1.0^\circ \pm 0.6^\circ$  enclosed with the BLG lattice. The buckling of BLG is  $119 \pm 1$  pm, which is similar to the corrugation of MLG and in accordance with previous work.<sup>105,108,110,111</sup> In BLG regions, the analysis of the moiré pattern yields a lattice constant of 0.248 nm and a rotation angle of  $0.33^\circ \pm 0.08^\circ$  with respect to Ru(0001) for the lower graphene layer. Within the uncertainty margins the values are comparable with those obtained for MLG and confirm that the moiré pattern of BLG on Ru(0001) is most likely due to the graphene–Ru(0001) interface.<sup>107,110,112</sup> A second moiré pattern was previously reported for BLG on Ru(0001) when elevated  $C_2H_4$  partial pressures were used for the graphene growth.<sup>108,109</sup> In the present experiments the  $C_2H_4$  partial pressure was two orders of magnitude lower than in the previous reports<sup>108,109</sup> and, therefore, most likely impeded the formation of the second moiré pattern.

Intercalation of Cs (Figure 2b) and Li (Figure 2c) starts in MLG regions, while BLG intercalation is only observed at saturation coverage (Figure 2c). In order to determine the corresponding intercalation structures, MLG on Ru(0001) cointercalated by Cs and Li (Figure 2d) is considered. The cointercalated sample exhibits domains of different apparent heights, where the characteristic buckling of MLG on Ru(0001) is strongly reduced. This observation evidences the successful intercalation of graphene with Cs and Li, which efficiently decouple MLG from the Ru surface. Consequently, the plane domains are attributed to separate Cs and Li intercalation phases, MLG/Cs and MLG/Li. The phase separation is most likely due to the lower delamination energy of Li-intercalated MLG. It is energetically favorable to form compact Li islands with a decreased graphene–Ru distance compared to the formation of mixed Cs-Li phases where the graphene–Ru separation would be increased due to the larger size of Cs.

The alkali metal intercalation structures may be deduced from atomically resolved STM images. Figure 3a presents the transition between MLG/Cs and MLG/Li regions with a difference in the apparent height of  $\approx 0.13$  nm (inset to Figure 3a). The intercalant assemblies are best seen from the atomically resolved close-up views of Figure 3a. In Figure 3b the honeycomb lattice of MLG is visible together with a regular hexagonal array of depressions. As corroborated by the Fourier transform (inset to Figure 3b) the array reflects a  $(2 \times 2)$  lattice with respect to MLG. Alkali metals were previously shown to preferably adopt the central part of a C hexagon of graphite or graphene,<sup>113,114</sup> which is assumed here for MLG/Cs as well. This assumption is also reasonable with respect to the same conclusions drawn for a  $(2 \times 2)$ Cs lattice observed from Cs-intercalated MLG on Ir(111).<sup>48</sup> Due to the lattice

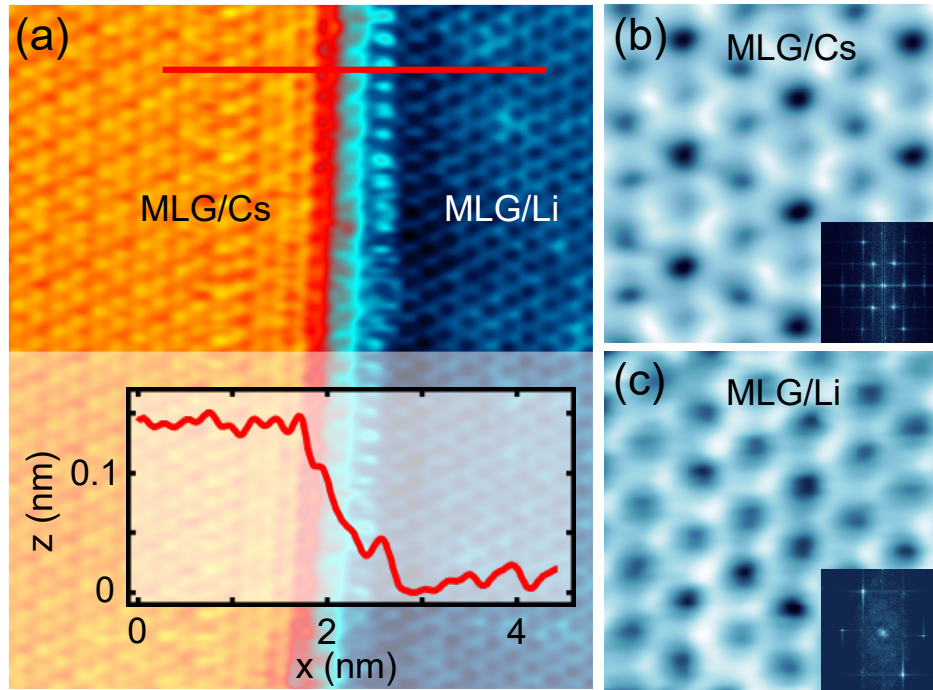


Figure 3: (Color online) Atomic structure of Cs and Li intercalation phases under MLG on Ru(0001). (a) STM image of adjacent Cs and Li intercalation phases (200 mV, 90 pA,  $5.5 \times 8 \text{ nm}^2$ ). Inset: Cross-sectional profile acquired along the line depicted in the top part of the STM image in (a). (b) Close-up view of Cs-intercalated domain with atomic resolution (200 mV, 90 pA,  $1.5 \times 1.5 \text{ nm}^2$ ). Inset: Fourier transform of (b) ( $11.9 \times 11.9 \text{ nm}^{-2}$ ) with outer spots reflecting the C lattice of MLG. The inner spots indicate the  $(2 \times 2)$ Cs ordered array. (c) Like (b) for a Li-intercalated region. Inset: Like the inset to (b) with identical spots for the MLG C lattice and the  $(1 \times 1)$ Li ordered structure.



mismatch between MLG and Ru(0001), the intercalated Cs atoms do not always occupy Ru on-top sites, which were demonstrated to be favored sites for the  $(2 \times 2)$ Cs superstructure on clean Ru(0001).<sup>77</sup>

Intercalation of Li under MLG on Ru(0001) leads to STM images as presented in Figure 3c. The MLG honeycomb lattice is visible only and a  $(1 \times 1)$ Li assembly with respect to the MLG lattice is inferred (inset to Figure 3c); that is, each C hexagon is occupied by a Li atom. An alternative explanation would be a disordered phase, which has recently been reported from room temperature photoemission experiments on Li-covered Ir(111) and Li-intercalated MLG on Ir(111).<sup>115</sup> However, at 5 K, which is the temperature of the experiments reported here, the suggested ordered  $(1 \times 1)$ Li intercalation phase is more plausible and agrees with the Li assembly observed at 6 K for Li-intercalated MLG on Ir(111).<sup>48</sup> For adsorption of Li on clean Ru(0001) a commensurate  $(\sqrt{3} \times \sqrt{3})R30^\circ$ -Li phase was discovered at low coverage with Li atoms preferably residing at threefold hcp hollow sites of Ru(0001).<sup>79</sup> At larger submonolayer coverage incommensurate superstructures occur where Li atoms adopt different adsorption sites.<sup>116</sup>

The intercalated  $(2 \times 2)$ Cs and  $(1 \times 1)$ Li phases observed here are formed with respect to the MLG lattice. Therefore, the preferred adsorption sites on clean Ru(0001) are no longer energetically favored, which demonstrates the strong impact of graphene on the energy landscape for alkali metal adsorption.

## Conclusions

Graphene can tune the atomic structure of intercalated phases. The observed equilibrium assembly reflects the balance between couplings of the intercalant with graphene, the substrate and other intercalants. Graphene on Pt(111) weakens the adsorption site specificity for intercalated Pt atoms and modifies the adsorption energy landscape. The resulting surface reconstruction exhibits qualitative changes in the underlying dislocation network as well as an increased regularity and extension compared to reconstructions of pristine Pt(111). The intercalation of Cs and Li on graphene-covered Ru(0001) unravels a stronger impact of graphene on the intercalant assembly. Alkali metal lattices form superstructures that are commensurate with the graphene lattice, irrespective of their substrate adsorption site. The findings of this work may spark the tailoring of surface structures by the presence of graphene.

## Acknowledgements

Financial support by the Deutsche Forschungsgemeinschaft through Grants No. KR 2912/10–1 and KR 2912/12 – 1 is acknowledged.

The authors declare no competing financial interest.

## References

- [1] Ibach, H. *Physics of surfaces and interfaces*; Springer, 2006.
- [2] Lüth, H. *Solid surfaces, interfaces and thin films*; Springer, 2015.
- [3] Barth, J.; Costantini, G.; Kern, K. Engineering atomic and molecular nanostructures at surfaces. *Nature* **2005**, *437*, 671 – 679.
- [4] Barth, J. V. Molecular Architectonic on Metal Surfaces. *Annu. Rev. Phys. Chem.* **2007**, *58*, 375–407.
- [5] Wang, Y.; Wu, K.; Kröger, J.; Berndt, R. Review Article: Structures of phthalocyanine molecules on surfaces studied by STM. *AIP Adv.* **2012**, *2*, 041402.
- [6] Shen, J.; Skomski, R.; Klaua, M.; Jenniches, H.; Manoharan, S. S.; Kirschner, J. Magnetism in one dimension: Fe on Cu(111). *Phys. Rev. B* **1997**, *56*, 2340–2343.
- [7] Gambardella, P.; Blanc, M.; Brune, H.; Kuhnke, K.; Kern, K. One-dimensional metal chains on Pt vicinal surfaces. *Phys. Rev. B* **2000**, *61*, 2254–2262.
- [8] Lin, J.-L.; Petrovykh, D. Y.; Kirakosian, A.; Rauscher, H.; Himpsel, F. J.; Dowben, P. A. Self-assembled Fe nanowires using organometallic chemical vapor deposition and CaF<sub>2</sub> masks on stepped Si(111). *Appl. Phys. Lett.* **2001**, *78*, 829–831.
- [9] Repain, V.; Baudot, G.; Ellmer, H.; Rousset, S. Two-dimensional long-range-ordered growth of uniform cobalt nanostructures on a Au(111) vicinal template. *EPL (Europhysics Letters)* **2002**, *58*, 730 – 736.
- [10] Kuhnke, K.; Kern, K. Vicinal metal surfaces as nanotemplates for the growth of low-dimensional structures. *J. Phys.: Condens. Matter* **2003**, *15*, S3311.
- [11] Néel, N.; Kröger, J.; Berndt, R. Highly Periodic Fullerene Nanomesh. *Adv. Mater.* **2006**, *18*, 174–177.
- [12] Néel, N.; Kröger, J.; Berndt, R. Fullerene nanowires on a vicinal gold surface. *Appl. Phys. Lett.* **2006**, *88*, 163101.
- [13] Kröger, J.; Jensen, H.; Néel, N.; Berndt, R. Self-organization of cobalt-phthalocyanine on a vicinal gold surface revealed by scanning tunnelling microscopy. *Surf. Sci.* **2007**, *601*, 4180–4184.
- [14] Chung, H. V.; Klevenz, M.; Lovrincic, R.; Neubrech, F.; Skibbe, O.; Pucci, A.; Nita, P.; Jalochofski, M.; Nagao, T. Studies on gold atom chains and lead nanowires on silicon vicinal surfaces. *J. Phys. Conf. Ser.* **2009**, *187*, 012025.

- [15] Barth, J. V.; Weckesser, J.; Cai, C.; Günter, P.; Bürgi, L.; Jeandupeux, O.; Kern, K. Building Supramolecular Nanostructures at Surfaces by Hydrogen Bonding. *Angew. Chem. Int. Ed.* **2000**, *39*, 1230–1234.
- [16] Theobald, J. A.; Oxtoby, N. S.; Phillips, M. A.; Champness, N. R.; Beton, P. H. Controlling molecular deposition and layer structure with supramolecular surface assemblies. *Nature* **2003**, *424*, 1029 – 1031.
- [17] Corso, M.; Auwärter, W.; Muntwiler, M.; Tamai, A.; Greber, T.; Osterwalder, J. Boron Nitride Nanomesh. *Science* **2004**, *303*, 217–220.
- [18] Dil, H.; Lobo-Checa, J.; Laskowski, R.; Blaha, P.; Berner, S.; Osterwalder, J.; Greber, T. Surface Trapping of Atoms and Molecules with Dipole Rings. *Science* **2008**, *319*, 1824–1826.
- [19] Berner, S.; Corso, M.; Widmer, R.; Groening, O.; Laskowski, R.; Blaha, P.; Schwarz, K.; Goriachko, A.; Over, H.; Gsell, S.; Schreck, M.; Sachdev, H.; Greber, T.; Osterwalder, J. Boron Nitride Nanomesh: Functionality from a Corrugated Monolayer. *Angew. Chem. Int. Ed.* **2007**, *46*, 5115–5119.
- [20] Goriachko, A.; He, Y. B.; Knapp, M.; Over, H.; Corso, M.; Brugger, T.; Berner, S.; Osterwalder, J.; Greber, T. Self-Assembly of a Hexagonal Boron Nitride Nanomesh on Ru(0001). *Langmuir* **2007**, *23*, 2928–2931.
- [21] Goriachko, A.; He, Y. B.; Over, H. Complex Growth of NanoAu on BN Nanomeshes Supported by Ru(0001). *J. Phys. Chem. C* **2008**, *112*, 8147–8152.
- [22] Järvinen, P.; Hämäläinen, S. K.; Ijäs, M.; Harju, A.; Liljeroth, P. Self-Assembly and Orbital Imaging of Metal Phthalocyanines on a Graphene Model Surface. *J. Phys. Chem. C* **2014**, *118*, 13320–13325.
- [23] Mao, J.; Zhang, H.; Jiang, Y.; Pan, Y.; Gao, M.; Xiao, W.; Gao, H.-J. Tunability of Supramolecular Kagome Lattices of Magnetic Phthalocyanines Using Graphene-Based Moiré Patterns as Templates. *J. Am. Chem. Soc.* **2009**, *131*, 14136–14137.
- [24] N’Diaye, A. T.; Gerber, T.; Busse, C.; Mysliveček, J.; Coraux, J.; Michely, T. A versatile fabrication method for cluster superlattices. *New J. Phys.* **2009**, *11*, 103045.
- [25] Pan, Y.; Gao, M.; Huang, L.; Liu, F.; Gao, H.-J. Directed self-assembly of monodispersed platinum nanoclusters on graphene Moiré template. *Appl. Phys. Lett.* **2009**, *95*, 093106.
- [26] Donner, K.; Jakob, P. Structural properties and site specific interactions of Pt with the graphene/Ru(0001) moiré overlayer. *The Journal of Chemical Physics* **2009**, *131*, 164701.

- [27] Cavallin, A.; Pozzo, M.; Africh, C.; Baraldi, A.; Vesselli, E.; Dri, C.; Comelli, G.; Larciprete, R.; Lacovig, P.; Lizzit, S.; Alfè, D. Local Electronic Structure and Density of Edge and Facet Atoms at Rh Nanoclusters Self-Assembled on a Graphene Template. *ACS Nano* **2012**, *6*, 3034–3043.
- [28] Sicot, M.; Bouvron, S.; Zander, O.; Rüdiger, U.; Dedkov, Y. S.; Fonin, M. Nucleation and growth of nickel nanoclusters on graphene Moiré on Rh(111). *Appl. Phys. Lett.* **2010**, *96*, 093115.
- [29] Pollard, A. et al. Supramolecular Assemblies Formed on an Epitaxial Graphene Superstructure. *Angew. Chem. Int. Ed.* **2010**, *49*, 1794–1799.
- [30] Sutter, E.; Albrecht, P.; Wang, B.; Bocquet, M.-L.; Wu, L.; Zhu, Y.; Sutter, P. Arrays of Ru nanoclusters with narrow size distribution templated by monolayer graphene on Ru. *Surf. Sci.* **2011**, *605*, 1676 – 1684.
- [31] Roos, M.; Künzel, D.; Uhl, B.; Huang, H.-H.; Brandao Alves, O.; Hoster, H. E.; Gross, A.; Behm, R. J. Hierarchical Interactions and Their Influence upon the Adsorption of Organic Molecules on a Graphene Film. *J. Am. Chem. Soc.* **2011**, *133*, 9208–9211.
- [32] Lu, J.; Yeo, P. S. E.; Zheng, Y.; Yang, Z.; Bao, Q.; Gan, C. K.; Loh, K. P. Using the Graphene Moiré Pattern for the Trapping of C60 and Homoepitaxy of Graphene. *ACS Nano* **2012**, *6*, 944–950.
- [33] Bazarnik, M.; Brede, J.; Decker, R.; Wiesendanger, R. Tailoring Molecular Self-Assembly of Magnetic Phthalocyanine Molecules on Fe- and Co-Intercalated Graphene. *ACS Nano* **2013**, *7*, 11341–11349.
- [34] Schulz, F.; Drost, R.; Hämäläinen, S. K.; Liljeroth, P. Templated Self-Assembly and Local Doping of Molecules on Epitaxial Hexagonal Boron Nitride. *ACS Nano* **2013**, *7*, 11121–11128.
- [35] Järvinen, P.; Hämäläinen, S. K.; Banerjee, K.; Häkkinen, P.; Ijäs, M.; Harju, A.; Liljeroth, P. Molecular Self-Assembly on Graphene on SiO<sub>2</sub> and h-BN Substrates. *Nano Lett.* **2013**, *13*, 3199–3204.
- [36] Banerjee, K.; Kumar, A.; Canova, F. F.; Kezilebieke, S.; Foster, A. S.; Liljeroth, P. Flexible Self-Assembled Molecular Templates on Graphene. *J. Phys. Chem. C* **2016**, *120*, 8772–8780.
- [37] Baltic, R.; Pivetta, M.; Donati, F.; Wäckerlin, C.; Singha, A.; Dreiser, J.; Rusponi, S.; Brune, H. Superlattice of Single Atom Magnets on Graphene. *Nano Lett.* **2016**, *16*, 7610–7615.

- [38] Avvisati, G.; Lisi, S.; Gargiani, P.; Pia, A. D.; Luca, O. D.; Pacilé, D.; Cardoso, C.; Varsano, D.; Prezzi, D.; Ferretti, A.; ; Betti, M. G. FePc Adsorption on the Moiré Superstructure of Graphene Intercalated with a Cobalt Layer. *J. Phys. Chem. C* **2017**, *121*, 1639–1647.
- [39] Pivetta, M.; Rusponi, S.; Brune, H. Direct capture and electrostatic repulsion in the self-assembly of rare-earth atom superlattices on graphene. *Phys. Rev. B* **2018**, *98*, 115417.
- [40] Kamna, M. M.; Stranick, S. J.; Weiss, P. S. Imaging Substrate-Mediated Interactions. *Science* **1996**, *274*, 118–119.
- [41] Wahlström, E.; Ekvall, I.; Olin, H.; Walldén, L. Long-range interaction between adatoms at the Cu(111) surface imaged by scanning tunnelling microscopy. *Appl. Phys. A* **1998**, *66*, 1107–1110.
- [42] Repp, J.; Moresco, F.; Meyer, G.; Rieder, K.-H.; Hyldgaard, P.; Persson, M. Substrate Mediated Long-Range Oscillatory Interaction between Adatoms: Cu /Cu(111). *Phys. Rev. Lett.* **2000**, *85*, 2981–2984.
- [43] Knorr, N.; Brune, H.; Epple, M.; Hirstein, A.; Schneider, M. A.; Kern, K. Long-range adsorbate interactions mediated by a two-dimensional electron gas. *Phys. Rev. B* **2002**, *65*, 115420.
- [44] Hyldgaard, P.; Persson, M. Long-ranged adsorbate-adsorbate interactions mediated by a surface-state band. *J. Phys.: Condens. Matter* **2000**, *12*, L13 – L19.
- [45] Silly, F.; Pivetta, M.; Ternes, M.; Patthey, F.; Pelz, J. P.; Schneider, W.-D. Creation of an Atomic Superlattice by Immersing Metallic Adatoms in a Two-Dimensional Electron Sea. *Phys. Rev. Lett.* **2004**, *92*, 016101.
- [46] Gopakumar, T.; Néel, N.; Kröger, J.; Berndt, R. Spatial modulation of d states in a nanoscale Co island. *Chem. Phys. Lett.* **2009**, *484*, 59–63.
- [47] Sutter, P. W.; Flege, J.-I.; Sutter, E. A. Epitaxial graphene on ruthenium. *Nat. Mater.* **2008**, *7*, 406.
- [48] Petrović, M. et al. The mechanism of caesium intercalation of graphene. *Nat. Commun.* **2013**, *4*, 2772.
- [49] Halle, J.; Néel, N.; Kröger, J. Filling the Gap: Li-Intercalated Graphene on Ir(111). *J. Phys. Chem. C* **2016**, *120*, 5067–5073.
- [50] Halle, J.; Néel, N.; Fonin, M.; Brandbyge, M.; Kröger, J. Understanding and Engineering Phonon-Mediated Tunneling into Graphene on Metal Surfaces. *Nano Lett.* **2018**, *18*, 5697–5701.

- [51] Franz, D.; Blanc, N.; Coraux, J.; Renaud, G.; Runte, S.; Gerber, T.; Busse, C.; Michely, T.; Feibelman, P. J.; Hejral, U.; Stierle, A. Atomic structure of Pt nanoclusters supported by graphene/Ir(111) and reversible transformation under CO exposure. *Phys. Rev. B* **2016**, *93*, 045426.
- [52] Horcas, I.; Fernández, R.; Gómez-Rodríguez, J. M.; Colchero, J.; Gómez-Herrero, J.; Baro, A. M. WSXM: A software for scanning probe microscopy and a tool for nanotechnology. *Rev. Sci. Instrum.* **2007**, *78*, 013705.
- [53] Sandy, A. R.; Mochrie, S. G. J.; Zehner, D. M.; Grübel, G.; Huang, K. G.; Gibbs, D. Reconstruction of the Pt(111) surface. *Phys. Rev. Lett.* **1992**, *68*, 2192–2195.
- [54] Grübel, G.; Huang, K. G.; Gibbs, D.; Zehner, D. M.; Sandy, A. R.; Mochrie, S. G. J. Reconstruction of the Pt(111) surface: X-ray-scattering measurements. *Phys. Rev. B* **1993**, *48*, 18119–18139.
- [55] Bott, M.; Hohage, M.; Michely, T.; Comsa, G. Pt(111) reconstruction induced by enhanced Pt gas-phase chemical potential. *Phys. Rev. Lett.* **1993**, *70*, 1489–1492.
- [56] Kontorova, T.; Frenkel, J. On the theory of plastic deformation and twinning. II. *Zh. Eksp. Teor. Fiz.* **1938**, *8*, 1340–1348.
- [57] Pushpa, R.; Narasimhan, S. Reconstruction of Pt(111) and domain patterns on close-packed metal surfaces. *Phys. Rev. B* **2003**, *67*, 205418.
- [58] Harten, U.; Lahee, A. M.; Toennies, J. P.; Wöll, C. Observation of a Soliton Reconstruction of Au(111) by High-Resolution Helium-Atom Diffraction. *Phys. Rev. Lett.* **1985**, *54*, 2619–2622.
- [59] Wöll, C.; Chiang, S.; Wilson, R. J.; Lippel, P. H. Determination of atom positions at stacking-fault dislocations on Au(111) by scanning tunneling microscopy. *Phys. Rev. B* **1989**, *39*, 7988–7991.
- [60] Barth, J. V.; Brune, H.; Ertl, G.; Behm, R. J. Scanning tunneling microscopy observations on the reconstructed Au(111) surface: Atomic structure, long-range superstructure, rotational domains, and surface defects. *Phys. Rev. B* **1990**, *42*, 9307–9318.
- [61] Narasimhan, S.; Vanderbilt, D. Elastic stress domains and the herringbone reconstruction on Au(111). *Phys. Rev. Lett.* **1992**, *69*, 1564–1567.
- [62] Grütter, P.; Dürig, U. Quasidendritic growth of Co induced by localized reconstruction of Pt(111). *Surf. Sci.* **1995**, *337*, 147 – 152.
- [63] Zhang, L.; van Ek, J.; Diebold, U. Highly ordered nanoscale surface alloy formed through Cr-induced Pt(111) reconstruction. *Phys. Rev. B* **1998**, *57*, R4285–R4288.
- [64] Holst, B.; Nohlen, M.; Wandelt, K.; Allison, W. Observation of an adlayer-driven substrate reconstruction in Cu-Pt(111). *Phys. Rev. B* **1998**, *58*, R10195–R10198.

- [65] Hohage, M.; Michely, T.; Comsa, G. Pt(111) network reconstruction: structure, growth and decay. *Surf. Sci.* **1995**, *337*, 249 – 267.
- [66] Merino, P.; Švec, M.; Pinaridi, A. L.; Otero, G.; Martín-Gago, J. A. Strain-Driven Moiré Superstructures of Epitaxial Graphene on Transition Metal Surfaces. *ACS Nano* **2011**, *5*, 5627–5634.
- [67] Gao, M.; Pan, Y.; Huang, L.; Hu, H.; Zhang, L. Z.; Guo, H. M.; Du, S. X.; Gao, H.-J. Epitaxial growth and structural property of graphene on Pt(111). *Appl. Phys. Lett.* **2011**, *98*, 033101.
- [68] Bonzel, H. P., Bradshaw, A. M., Ertl, G., Eds. *Physics and chemistry of alkali metal adsorption*; Elsevier, 1989.
- [69] Diehl, R. D.; McGrath, R. Structural studies of alkali metal adsorption and coadsorption on metal surfaces. *Surf. Sci. Rep.* **1996**, *23*, 43 – 171.
- [70] Diehl, R. D.; McGrath, R. Current progress in understanding alkali metal adsorption on metal surfaces. *J. Phys.: Condens. Matter* **1997**, *9*, 951 – 968.
- [71] Ortega, J. E.; Oellig, E. M.; Ferrón, J.; Miranda, R. Cs and O adsorption on Si(100)  $2 \times 1$ : A model system for promoted oxidation of semiconductors. *Phys. Rev. B* **1987**, *36*, 6213–6216.
- [72] Tikhov, M.; Rangelov, G.; Surnev, L. Interaction of oxygen with Na-covered Si(100). *Surf. Sci.* **1990**, *231*, 280 – 288.
- [73] Faraci, G.; Pennisi, A. Ge(100)  $2 \times 1$  substoichiometric oxidation states promoted by a Cs overlayer. *Surf. Sci.* **1998**, *409*, 46 – 56.
- [74] Davydov, S. Y. On the interaction of oxygen with a Cs-monolayer-covered Si(100) surface. *Appl. Surf. Sci.* **1999**, *140*, 58 – 62.
- [75] Taylor, J. B.; Langmuir, I. The Evaporation of Atoms, Ions and Electrons from Caesium Films on Tungsten. *Phys. Rev.* **1933**, *44*, 423–458.
- [76] Lindgren, S. A.; Walldén, L.; Rundgren, J.; Westrin, P.; Neve, J. Structure of Cu(111) $p(2 \times 2)$ Cs determined by low-energy electron diffraction. *Phys. Rev. B* **1983**, *28*, 6707–6712.
- [77] Over, H.; Bludau, H.; Skottke-Klein, M.; Ertl, G.; Moritz, W.; Campbell, C. T. Coverage dependence of adsorption-site geometry in the Cs/Ru(0001) system: A low-energy electron-diffraction analysis. *Phys. Rev. B* **1992**, *45*, 8638–8649.
- [78] Leatherman, G. S.; Diehl, R. D. Phase diagrams and rotated incommensurate phases of K, Rb, and Cs adsorbed on Ag(111). *Phys. Rev. B* **1996**, *53*, 4939–4946.

- [79] Gierer, M.; Over, H.; Bludau, H.; Ertl, G. Structural properties of ordered alkali metal overlayers: a LEED analysis of the Ru(0001)-( $\sqrt{3} \times \sqrt{3}$ )R30°-Li phase in comparison with related systems. *Surf. Sci.* **1995**, *337*, 198 – 204.
- [80] von Hofe, T.; Kröger, J.; Berndt, R. Adsorption geometry of Cu(111)–Cs studied by scanning tunneling microscopy. *Phys. Rev. B* **2006**, *73*, 245434.
- [81] Ziegler, M.; Kröger, J.; Berndt, R.; Filinov, A.; Bonitz, M. Scanning tunneling microscopy and kinetic Monte Carlo investigation of cesium superlattices on Ag(111). *Phys. Rev. B* **2008**, *78*, 245427.
- [82] He, P.; Jacobi, K. Vibrational analysis of cesium on Ru(0001). *Phys. Rev. B* **1996**, *53*, 3658–3661.
- [83] Rusina, G. G.; Ereemeev, S. V.; Echenique, P. M.; Benedek, G.; Borisova, S. D.; Chulkov, E. V. Vibrations of alkali metal overlayers on metal surfaces. *J. Phys.: Condens. Matter* **2008**, *20*, 224007.
- [84] Kröger, J.; Bruchmann, D.; Lehwald, S.; Ibach, H. Adsorption of lithium on Mo(110): an EELS study of the adsorbate vibrations and substrate phonons. *Surf. Sci.* **2000**, *449*, 227 – 235.
- [85] Kröger, J.; Lehwald, S.; Ibach, H. Surface dynamics of Mo(110)-H and Mo(110)-Li. *Surf. Sci.* **2003**, *530*, 170 – 174.
- [86] Bauer, M.; Pawlik, S.; Aeschlimann, M. Resonance lifetime and energy of an excited Cs state on Cu(111). *Phys. Rev. B* **1997**, *55*, 10040–10043.
- [87] Ogawa, S.; Nagano, H.; Petek, H. Phase and Energy Relaxation in an Antibonding Surface State: Cs/Cu(111). *Phys. Rev. Lett.* **1999**, *82*, 1931–1934.
- [88] Borisov, A. G.; Gauyacq, J. P.; Kazansky, A. K.; Chulkov, E. V.; Silkin, V. M.; Echenique, P. M. Long-Lived Excited States at Surfaces: Cs/Cu(111) and Cs/Cu(100) Systems. *Phys. Rev. Lett.* **2001**, *86*, 488–491.
- [89] Gauyacq, J.; Borisov, A.; Kazansky, A. Impurity-induced localisation of the 2D surface-state continuum on a metal surface. *Appl. Phys. A* **2004**, *78*, 141–147.
- [90] Corriol, C.; Silkin, V. M.; Sánchez-Portal, D.; Arnau, A.; Chulkov, E. V.; Echenique, P. M.; von Hofe, T.; Kliewer, J.; Kröger, J.; Berndt, R. Role of Elastic Scattering in Electron Dynamics at Ordered Alkali Overlayers on Cu(111). *Phys. Rev. Lett.* **2005**, *95*, 176802.
- [91] Kröger, J.; Becker, M.; Jensen, H.; von Hofe, T.; Néel, N.; Limot, L.; Berndt, R.; Crampin, S.; Pehlke, E.; Corriol, C.; Silkin, V.; Sánchez-Portal, D.; Arnau, A.; Chulkov, E.; Echenique, P. Dynamics of surface-localised electronic excitations studied with the scanning tunnelling microscope. *Prog. Surf. Sci.* **2007**, *82*, 293 – 312.



- [92] Ziegler, M.; Kröger, J.; Berndt, R.; Borisov, A. G.; Gauyacq, J. P. Linewidth of a cesium adatom resonance on Ag(111). *Phys. Rev. B* **2009**, *79*, 075401.
- [93] Papagno, M.; Rusponi, S.; Sheverdyeva, P. M.; Vlais, S.; Etzkorn, M.; Pacilé, D.; Moras, P.; Carbone, C.; Brune, H. Large Band Gap Opening between Graphene Dirac Cones Induced by Na Adsorption onto an Ir Superlattice. *ACS Nano* **2012**, *6*, 199–204.
- [94] Matyba, P.; Carr, A.; Chen, C.; Miller, D. L.; Peng, G.; Mathias, S.; Mavrikakis, M.; Dessa, D. S.; Keller, M. W.; Kapteyn, H. C.; Murnane, M. Controlling the electronic structure of graphene using surface-adsorbate interactions. *Phys. Rev. B* **2015**, *92*, 041407(R).
- [95] Chen, J.-H.; Jang, C.; Adam, S.; Fuhrer, M. S.; Williams, E. D.; Ishigami, M. Charged-impurity scattering in graphene. *Nat. Phys.* **2008**, *4*, 377 – 381.
- [96] Woo, S.; Hemmatiyani, S.; Morrison, T. D.; Rathnayaka, K. D. D.; Lyuksyutov, I. F.; Naugle, D. G. Temperature-dependent transport properties of graphene decorated by alkali metal adatoms (Li, K). *Appl. Phys. Lett.* **2017**, *111*, 263502.
- [97] Schumacher, S.; Wehling, T. O.; Lazić, P.; Runte, S.; Förster, D. F.; Busse, C.; Petrović, M.; Kralj, M.; Blügel, S.; Atodiresei, N.; Caciuc, V.; Michely, T. The Backside of Graphene: Manipulating Adsorption by Intercalation. *Nano Lett.* **2013**, *13*, 5013–5019.
- [98] Profeta, G.; Calandra, M.; Mauri, F. Phonon-mediated superconductivity in graphene by lithium deposition. *Nat. Phys.* **2012**, *8*, 131 – 134.
- [99] McChesney, J. L.; Bostwick, A.; Ohta, T.; Seyller, T.; Horn, K.; González, J.; Rotenberg, E. Extended van Hove Singularity and Superconducting Instability in Doped Graphene. *Phys. Rev. Lett.* **2010**, *104*, 136803.
- [100] Ludbrook, B. M. et al. Evidence for superconductivity in Li-decorated monolayer graphene. *Proceedings of the National Academy of Sciences* **2015**, *112*, 11795–11799.
- [101] Wang, B.; Bocquet, M.-L.; Marchini, S.; Günther, S.; Wintterlin, J. Chemical origin of a graphene moire overlayer on Ru(0001). *Phys. Chem. Chem. Phys.* **2008**, *10*, 3530–3534.
- [102] Preobrajenski, A. B.; Ng, M. L.; Vinogradov, A. S.; Mårtensson, N. Controlling graphene corrugation on lattice-mismatched substrates. *Phys. Rev. B* **2008**, *78*, 073401.
- [103] Jiang, D.-e.; Du, M.-H.; Dai, S. First principles study of the graphene/Ru(0001) interface. *J. Chem. Phys.* **2009**, *130*, 074705.
- [104] Marchini, S.; Günther, S.; Wintterlin, J. Scanning tunneling microscopy of graphene on Ru(0001). *Phys. Rev. B* **2007**, *76*, 075429.
- [105] Sutter, E.; Acharya, D. P.; Sadowski, J. T.; Sutter, P. Scanning tunneling microscopy on epitaxial bilayer graphene on ruthenium (0001). *Appl. Phys. Lett.* **2009**, *94*, 133101.

- [106] Altenburg, S. J.; Kröger, J.; Wang, B.; Bocquet, M.-L.; Lorente, N.; Berndt, R. Graphene on Ru(0001): Contact Formation and Chemical Reactivity on the Atomic Scale. *Phys. Rev. Lett.* **2010**, *105*, 236101.
- [107] Que, Y.; Xiao, W.; Fei, X.; Chen, H.; Huang, L.; Du, S. X.; Gao, H.-J. Epitaxial growth of large-area bilayer graphene on Ru(0001). *Appl. Phys. Lett.* **2014**, *104*, 093110.
- [108] Papagno, M. et al. Two Distinct Phases of Bilayer Graphene Films on Ru(0001). *ACS Nano* **2012**, *6*, 9299–9304.
- [109] Dubout, Q.; Calleja, F.; Schlauzero, G.; Etzkorn, M.; Lehnert, A.; Claude, L.; Papagno, M.; Natterer, F. D.; Patthey, F.; Rusponi, S.; Pasquarello, A.; Brune, H. Giant apparent lattice distortions in STM images of corrugated  $sp^2$ -hybridised monolayers. *New J. Phys.* **2016**, *18*, 103027.
- [110] Wang, B.; Bocquet, M.-L. Interfacial coupling in rotational monolayer and bilayer graphene on Ru(0001) from first principles. *Nanoscale* **2012**, *4*, 4687–4693.
- [111] Moritz, W.; Wang, B.; Bocquet, M.-L.; Brugger, T.; Greber, T.; Wintterlin, J.; Günther, S. Structure Determination of the Coincidence Phase of Graphene on Ru(0001). *Phys. Rev. Lett.* **2010**, *104*, 136102.
- [112] Cui, Y.; Fu, Q.; Bao, X. Dynamic observation of layer-by-layer growth and removal of graphene on Ru(0001). *Phys. Chem. Chem. Phys.* **2010**, *12*, 5053–5057.
- [113] DiVincenzo, D. P.; Mele, E. J. Cohesion and structure in stage-1 graphite intercalation compounds. *Phys. Rev. B* **1985**, *32*, 2538–2553.
- [114] Uthaisar, C.; Barone, V. Edge Effects on the Characteristics of Li Diffusion in Graphene. *Nano Lett.* **2010**, *10*, 2838–2842.
- [115] Pervan, P.; Lazić, P.; Petrović, M.; Šrut Rakić, I.; Pletikosić, I.; Kralj, M.; Milun, M.; Valla, T. Li adsorption versus graphene intercalation on Ir(111): From quenching to restoration of the Ir surface state. *Phys. Rev. B* **2015**, *92*, 245415.
- [116] Gierer, M.; Over, H.; Bludau, H.; Ertl, G. Incommensurate structures and epitaxial growth of Li on Ru(0001): A quantitative low-energy electron-diffraction study. *Phys. Rev. B* **1995**, *52*, 2927–2934.